Electronic Supporting Information (ESI)

Prediction of Allotropes of Tellurium with Molecular, one- and two-dimensional Covalent Nets for Photofunctional Applications

Heng Zhang[1,2], Junjie Wang[1]*, Frédéric Guegan[2], Shuyin Yu[3], Gilles Frapper[2,1]*

[1]State Key Laboratory of Solidification Processing and International Center for Materials Discovery, School of Materials Science and Engineering, Northwestern Polytechnical University, Xi'an, Shaanxi 710072, People's Republic of China.

[2]Applied Quantum Chemistry group, E4, IC2MP, UMR 7285 Poitiers university-CNRS, 4 rue Michel Brunet TSA 51106 - 86073 Poitiers Cedex 9, France.

[3]MSEA International Institute for Materials Genome, Jinxiu Rd. 1, Gu'an, Hebei 065500, People's Republic of China

*Corresponding author. Email: wang.junjie@nwpu.edu.cn

gilles.frapper@univ-poitiers.fr

CONTENTS

S1 Methodology

S1.1 Evolutionary algorithm (USPEX)

USPEX (Universal Structure Predictor: Evolutionary Xtallography) is a global evolutionary search algorithm for crystal structure prediction developed by the A.R. Oganov laboratory since 2004 (see http://uspex-team.org/en/uspex/overview).[1-3] In this work, this evolutionary algorithm (EA) code is interfaced with VASP (Vienna Ab initio Simulation Package) for DFT structure relaxation (shape, volume, atomic positions are optimized by VASP).[4,5] The EA development allows the prediction of the stable and metastable structures knowing only the chemical composition at zero Kelvin, e.g., Te. Simultaneous searches for stable compositions and structures are also possible; For the resulting Te minimum, a fixed composition on the bulk and 2D materials is then employed to locate the most stable structure. The EA search is performed at least twice to ensure convergence to a global minimum. In our fixed-composition USPEX calculations on bulk Te, the total number of atoms per unit cell is in the limitation of 32. Especially, for 2D fixed-composition calculations, the atom number per unit cell is in the range of 2-12, the initial thickness of 2D Te is set to 1.5 Å and the vacuum size is 20 Å.

A large number (100) of randomly created structures is chosen in the first generation of the EA. In the next generations, 80 structures are generated. What is the generation process? For each parent structure from a previous generation, the fitness is computed as the free enthalpy derived from an ab initio total energy calculation (here VASP). All structures are then tested against three constraints: interatomic distances, cell angles and cell lengths. 80% of the best (i.e. lowest enthalpy) optimized structures are selected to participate in producing the next generation. new candidate structure is produced from parent structures using one of four operators defined in Refs 1-3: (i) heredity, (ii) lattice mutations, and (iii) atomic mutation, which account for 50, 10, and 20% of the structures in the new generation. The remaining 20% are randomly generated (similarly to those of the first generation). A fixed composition EA search is considered achieved when the same global structure minimum is found during 10 consecutive generations. Typically, such search requires between 10 and 20 generations. The seeds technology in USPEX is used during CSP searches.[6]

S1.2 DFT calculations (VASP)

First-principles calculations are performed using the projected-augmented-wave (PAW) method as implemented in VASP (version 5.4.4).[7] Exchange-correlation energy is treated using

Perdew-Burke-Ernzerhof (PBE) within the generalized gradient approximation (GGA).[8,9] A kinetic cutoff energy of 600 eV is used for the wavefunction expansion with a Monkhorst-Pack k mesh grid with a spacing of $2\pi \times 0.04$ Å^{-1}. This ensure that enthalpy converges to a criterion lower than 1×10^{-5} eV per cell. In USPEX calculation, 5 successive steps of increasing convergence accuracy are usually required (ie.5 INCAR files). An illustration of this local optimization procedure is given in the PhD manuscript of B. Huang, "Computational materials discovery: prediction of carbon dioxide and nitrogen-based compounds under pressure using density functional theory and evolutionary algorithm", supervised by Pr. G. Frapper, IC2MP, Poitiers University (France), Dec. 2017 http://theses.univ-poitiers.fr/notice/view/59262). The parameters and criterion associated with VASP calculations then correspond to the last (5th) step of the highest accuracy.

Ab initio molecular dynamics (AIMD) simulations based on DFT were carried out using VASP code to examine the thermal stability of 2D Te phases. AIMD calculations were performed up to 500 K. The timestep was 2 fs, and the total simulation time was as long as 12 ps. In such AIMD simulations, 4×4 supercells were employed, and the Brillouin zone integration was restricted to the Γ point of the supercell, due to a high calculation cost.

S1.2 Phonon and zero-point energy calculations

In this work, first principles phonon calculations with density functional perturbation theory (DFPT) at quasi-harmonic level were done using the open-source package PHONOPY (https://atztogo.github.io/phonopy/).[10] Supercell structures with displacements were created from a unit cell fully considering crystal symmetry. In general, a 3x3 supercell is needed, sometimes higher.

The zero-point energy (ZPE) factor was calculated from the computed phonon frequencies ω_i under the quasi-harmonic approximation. ZPE is proportional to the sum over all phonon modes ω_i (k-points and branches). The detailed theoretical methodology implemented in PHONOPY code is given in reference 10 and references therein. The calculated ZPEs are listed in Tables S1, S3 and S6.

S1.3 Mechanical properties

A necessary condition for the thermodynamic stability of a crystal lattice is that the crystal should be mechanically stable with respect to arbitrary (small) homogeneous deformations. Elastic stability criteria for bulk cubic crystals and more different crystal classes was well understood in the work of Born and co-authors.[11-13] In VASP, IBRION=6 and ISIF≥3 tags allow to calculate the elastic constants. The elastic tensor is determined by performing six finite distortions of the lattice and deriving the elastic constants from the strain-stress relationship. [14]

The elastic matrix of 2D materials was decreased into 3×3 and six elastic constants are C_{11}, C_{12}, C_{22}, C_{16}, C_{26} and C_{66} using the standard Voigt notation:1-xx, 2-yy, 6-xy. In 2D rectangular unit-cells, C_{16} and C_{26} are zero. The calculated elastic constants C_{11}, C_{12}, C_{22} and C_{66} in 2D materials should satisfy necessary mechanical equilibrium conditions for mechanical stability: $C_{11}C_{22}$-$C_{12}C_{21}>0$ and C_{11}, C_{22}, $C_{66}>0$.[15]

S1.4 Carrier mobility

The intrinsic carrier mobility u of 2D crystals was investigated within the framework of the deformation potential theory for semiconductors proposed by Bardeen and Shockley.[16] In the long-wavelength limit, when only the interaction between electron and longitudinal acoustic phonon is taken into consideration, the carrier mobility of 2D crystals can be expressed by following formula,[17]

$$\mu = \frac{e\hbar^3 C_{2D}}{kTm^*_{e(h)}m^*_d E_l^2}, \qquad \text{(eq.1)}$$

in which e is electron charge, $\hbar$ is the reduced Planck's constant, T is temperature (300K in this work), $m^*_{e(h)}$ is effective mass of electron or hole determined by $m^*_{e(h)} = \frac{\hbar^2}{(\partial^2 E(k)/\partial k^2)}$, m^*_d is average effective mass along x and y directions defined by $(m^*_x m^*_y)^{1/2}$. The 2D elastic modulus C_{2D} of the longitudinal strain in the propagation directions (x, y) of the longitudinal acoustic wave was derived from $(E-E_0)/S_0 = C_{2D}(\Delta l/l_0)^2/2$, where E_0 and E are the total energies of 2D unstrained and strained crystals, S_0 is the equilibrium lattice area of 2D crystal, Δl is the small dilation of the lattice constant l_0 along the transport direction. E_l is the deformation potential constant, given by $E_l^{e(h)} = \Delta E_{CBM(VBM)}/(\Delta l/l_0)$ in which $\Delta E_{CBM(VBM)}$ is the energy shift of valence band maximum (VBM) and conduction band minimum (CBM) with respect to the vacuum level.

S2 Bulk Te allotropes at ambient condition

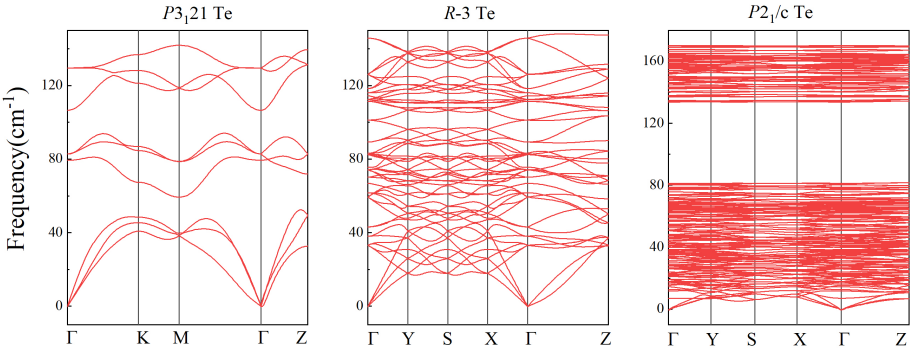

Fig. S1 Phonon dispersion curves of three Te allotropes, $P3_121$, R-3 and $P2_1/c$ Te phase.

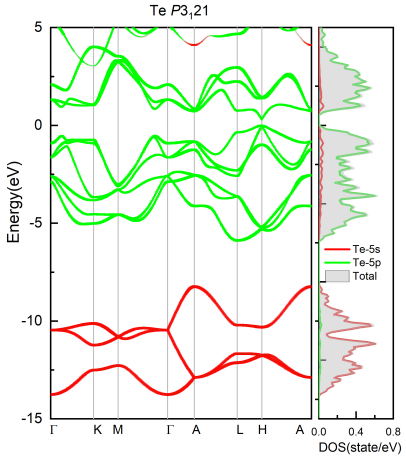

Fig. S2 Projected band structure and DOS of the ground-state $P3_121$ Te phase.

S3 2D Te phases

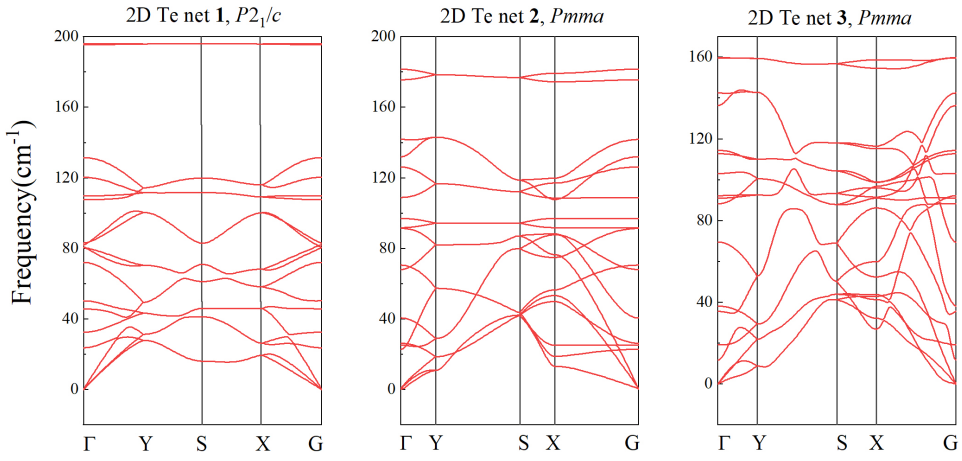

Fig. S3 Phonon dispersion curves of 2D Te phases, **1**, **2** and **3**.

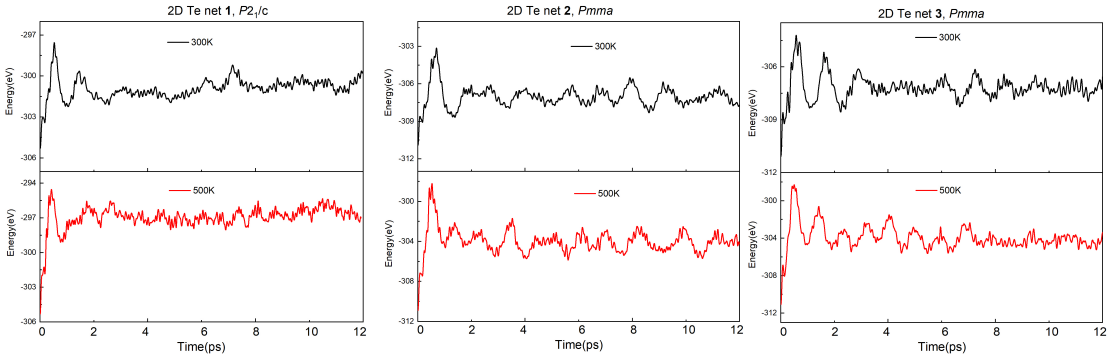

(a) (b) (c)

Fig. S4 Energy fluctuations of (a) 2D Te net **1**, (b) 2D Te net **2**, (c) 2D Te net **3** during the AIMD simulations at specific temperatures, T = 300K, 500K.

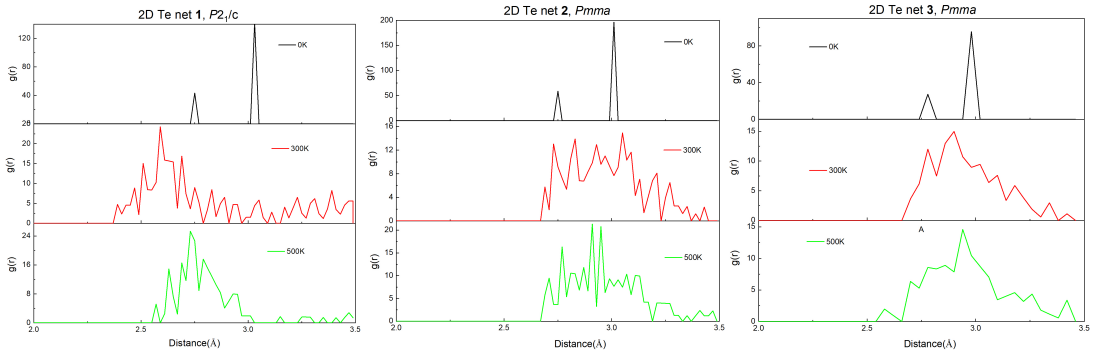

(a) (b) (c)

Fig. S5 Radial distribution functions (RDF) for the Te-Te separations observed during AIMD simulations at T = 0 K, 300 K, 500 K, (a) 2D Te net **1**, (b) 2D Te net **2**, (c) 2D Te net **3**.

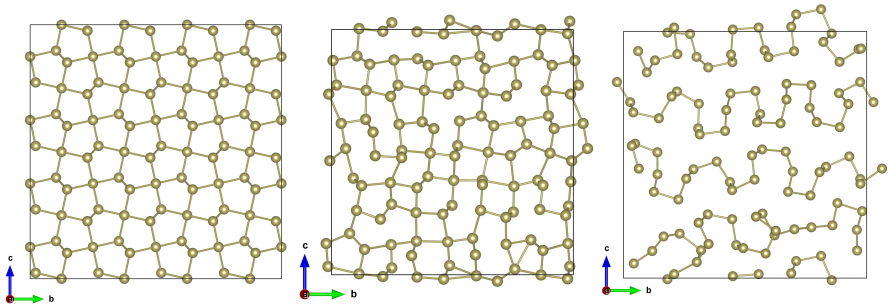

0K 300K 500K

Fig. S6 Snapshots of the 2D Te net **1** supercell (4×4) at ambient pressure at the end of 12 ps.

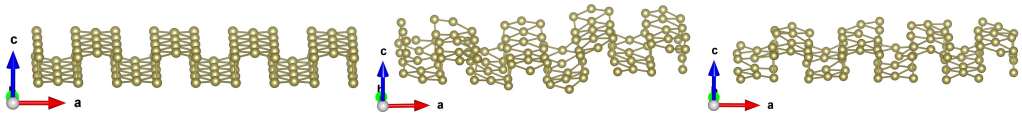

0K 300K 500K

Fig. S7 Snapshots of the 2D Te net **2** supercell (4×4) at ambient pressure at the end of 12 ps.

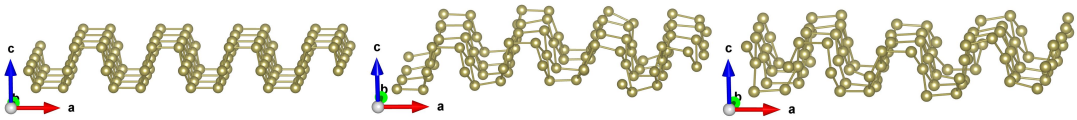

0K 300K 500K

Fig. S8 Snapshots of the 2D Te net **3** supercell (4×4) at ambient pressure at the end of 12 ps.

S4 Bulk layered materials

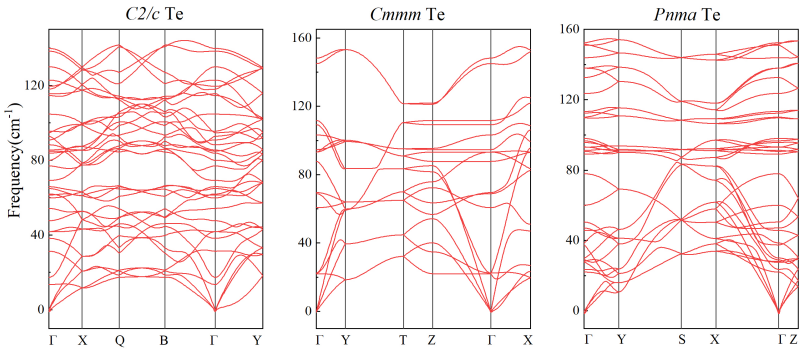

Fig. S9 Phonon dispersion curves of bulk layered Te allotropes.

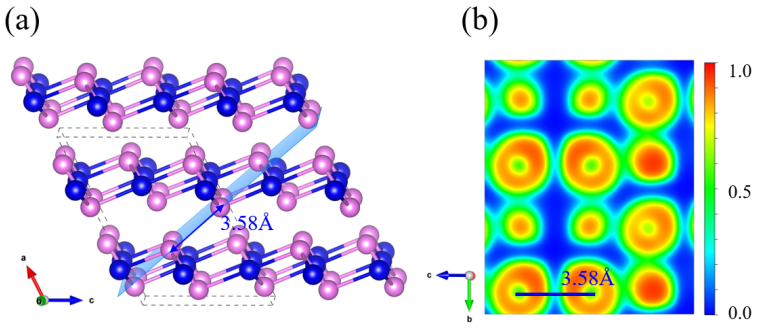

Fig. S10 (a) Structure configuration of **1_bulk** in which the $(20\bar{1})$ plane is depicted in light blue; (b) 2D ELF contour of **1_bulk** in $(20\bar{1})$ plane with the isosurface level 0.75.

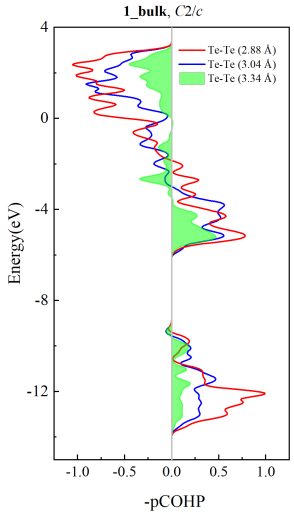

Fig. S11 pCOHP curve of Te-Te contacts in **1_bulk** *C*2/*c*. The bond distance is indicated in the parentheses.

S5 Partial charge distributions

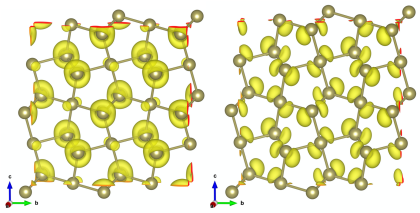

(a) (b)

Fig. S12 Partial charge distributions at (a) VBM and (b) CBM in the range 0.10 eV in 2D Te net **1**

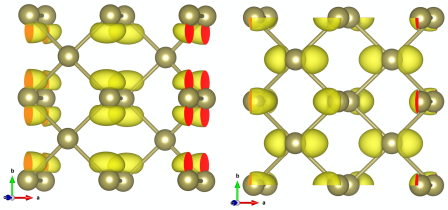

(a) (b)

Fig. S13 Partial charge distributions at (a) VBM and (b) CBM in the range 0.10 eV in 2D Te net **2**

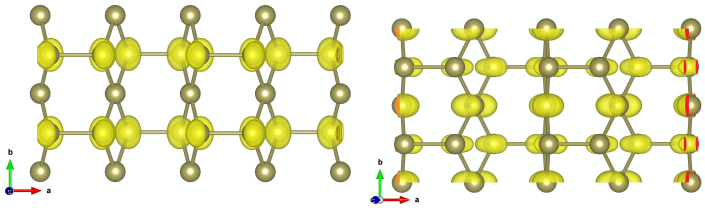

(a) (b)

Fig. S14 Partial charge distributions at (a) VBM and (b) CBM in the range 0.10 eV in 2D Te net **3**

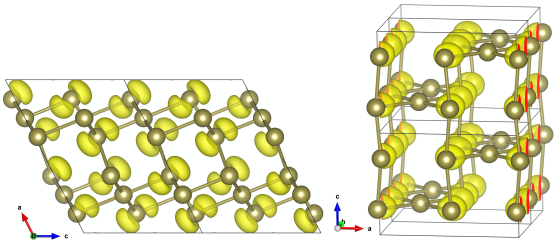

(a) (b)

Fig. S15 Partial charge distributions near the Fermi energy with the range ±0.05 eV in (a) **1_bulk** and (b) **2_bulk**.

S6 Optical absorptions

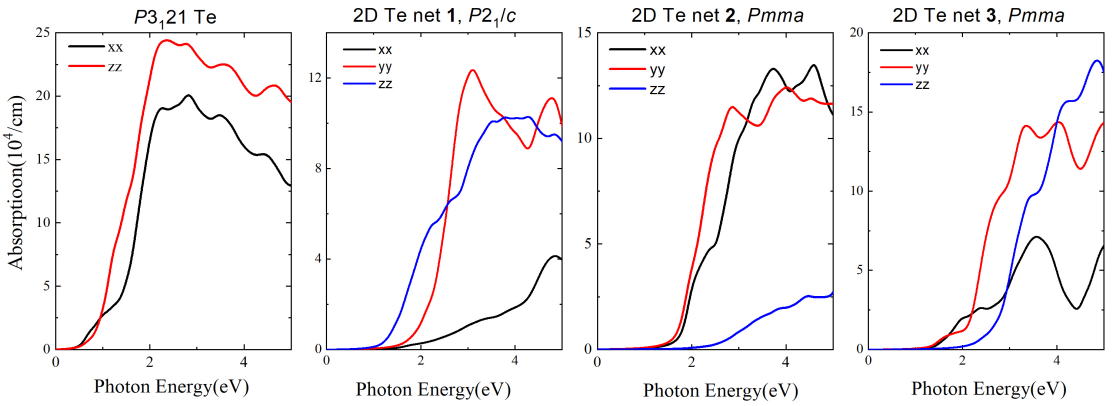

Fig. S16. The calculated optical absorptions of (a) bulk $P3_121$ Te and (b) 2D Te net **1**, (c) 2D Te net **2**, (d) 2D Te net **3** along different spatial directions.

The blue shifts of optical absorption in 2D Te structures were found in comparison with that of 3D bulk case, which is resulted from the decreased dimensionality. Also, the optical onsets of 2D Te structures are significantly different due to their various band gaps. A noteworthy difference between the optical response for light polarized along *a*, *b*, and *c* directions appears. This anisotropic phenomenon is determined by the selection rules associated with symmetries. Due to the large layer thickness, 2D Te net **3** shows a moderate optical absorption for the light polarization along *c* direction. What is more, semiconducting 2D Te nanosheets exhibit strong and prominent optical absorptions in the range of 1.5-4 eV for the light polarization along *a* and *b* directions, which covers the visible to ultraviolet light regime. For 2D Te structures, their prominent absorption peaks beyond the band gap in the visible regime are dominated by direct inter-band transitions at the high-symmetry *k*-point Γ.

S7 Enthalpies, structural parameters, and elastic constants

Table S1 Calculated enthalpies, ZPE of three bulk Te phases at ambient condition within PBE functional with D2 correction.

Phase	Z	Space Group	Enthalpy (eV/atom)	ZPE (eV/atom)
Te	3	$P3_121$ SG 152	-3.449	0.015
Te	18	R-3 SG 148	-3.428	0.015
Te	64	$P2_1/c$ SG 14	-3.351	0.015

Table S2 Structural parameters of the predicted Te bulk at ambient condition (distances in Å, angles in °) within PBE functional with D2 correction.

Phase	Z	Space Group	Lattice Parameter	Atomic coordinates (fractional)
Te	3	$P3_121$ SG 152	a=b=4.338, c=6.031 α=β=90.0, γ=120.0	3a (0.277, 0.000, 0.333)
Te	18	R-3 SG 148	a=b=12.221, c=4.595 α=β=90.0, γ=120.0	18f (0.034, 0.815, 0.160)
Te	64	$P2_1/c$ SG 14	a=16.358, b=16.035, c=9.173 α=γ=90.0, β=93.6	4e (0.017 0.085 0.299) 4e (0.024 0.727 0.366) 4e (0.090 0.147 0.706) 4e (0.093 0.526 0.618) 4e (0.163 0.638 0.997) 4e (0.192 0.182 0.485) 4e (0.207 0.540 0.242) 4e (0.223 0.710 0.614) 4e (0.251 0.987 0.250) 4e (0.323 0.082 0.036)

				4e (0.315 0.239 0.164) 4e (0.346 0.031 0.631) 4e (0.353 0.661 0.446) 4e (0.481 0.693 0.650) 4e (0.461 0.152 0.429) 4e (0.486 0.540 0.279)

Table S3 Calculated (formation) enthalpies, ZPE of 2D Te nets within PBE functional with D2 correction.

Phase	Z	Space Group	Enthalpy (eV/atom)	Formation Enthalpy (eV/atom)	ZPE (eV/atom)
α-Te	3	*P*-3*m*1 SG 164	-3.278	0.171	0.016
ξ-Te	3	*P*4/*mmm* SG 123	-3.277	0.172	0.015
3	6	*Pmma* SG 51	-3.247	0.202	0.016
2	6	*Pmma* SG 51	-3.241	0.208	0.016
β-Te	3	*P*2/*m* SG 10	-3.221	0.228	0.016
1	6	$P2_1/c$ *SG 14*	-3.181	0.268	0.016
square-Te	2	*P*4/*nmm* SG129	-3.153	0.296	0.013
γ-Te	3	*P*-6*m*2 SG187	-3.115	0.334	0.013

Table S4 Structural parameters of 2D Te nets (distances in Å, angles in °) within PBE functional with D2 correction.

Phase	Z	Space Group	Lattice parameter	Atomic coordinates (fractional)
α-Te	3	*P*-3*m*1 SG 164	a=b=4.151, c=23.669 α=β=90.0, γ=120.0	2d (0.333 0.667 0.922) 1a (0.000 0.000 0.000)
ξ-Te	3	*P*4/*mmm* SG 123	a=b=3.136, c=26.211 α=β=γ=90.0	2g (0.000 0.000 0.118) 1a (0.000 0.000 0.000)
3	6	*Pmma* SG 51	a=7.961, b=4.131, c=24.179 α=β=γ=90.0	4j (0.074 0.500 0.086) 2a (0.000 0.000 0.000)
η-Te*	6	$P222_1$ SG 17	a=4.423, b=29.667, c=8.521 α=β=γ=90.0[18]	4e (0.011 0.070 0.415) 2a (0.432 0.000 0.500)
2	6	*Pmma* SG 51	a=8.522, b=4.201, c=23.106 α=β=γ=90.0	4i (0.504 0.000 0.560) 2f (0.250 0.500 0.567)
δ-Te*	6	*Pma*2 SG 28	a=10.319, b=31.060, c=4.424 α=β=γ=90.0[18]	4d (0.036 0.956 0.470) 2c (0.250 0.958 0.047)
β-Te	3	*P*2/*m* SG 10	a=22.163, b=4.172, c=5.490 α=β=γ=90.0	2m (0.951 0.000 0.155) 1f (0.000 0.500 0.500)
1	6	$P2_1/c$ *SG14*	a=22.142, b=6.721, c=6.806 α=β=γ=90.0	4e (0.048 0.912 0.407) 2a (0.000 0.000 0.000)
square-Te	2	*P*4/*nmm* SG129	a=b=4.092, c=20.872 α=β=γ=90.0	2c (0.500 0.000 0.479)
γ-Te	3	*P*-6*m*2 SG187	a=b=3.939, c=24.138 α=β=90.0, γ=120.0	1d (0.333 0.667 0.500) 2g (0.000 0.000 0.586)

*The crystallographic parameters of η-Te and δ-Te phases were provided by Dan Liu and

coworkers.[18] When a full structural optimization was employed, the chains in η-Te and δ-Te phases would be bonded together and then transformed into 2D Te net **2** and **3** crystalizing in orthorhombic space group *Pmma*.

Table S5 Elastic constants C_{11}, C_{12}, C_{22}, C_{66} (GPa) in three 2D Te nets **1**, **2** and **3**.

	Space group	C_{11}	C_{12}	C_{22}	C_{66}
1	$P2_1/c$ *SG 14*	27.951	0.342	38.314	7.626
2	*Pmma* SG 51	17.033	8.093	44.817	10.263
3	*Pmma* SG 51	16.255	0.179	44.692	2.726

Table S6 Calculated enthalpy, ZPE of the proposed layered Te bulk allotropes within PBE functional with D2 correction.

Te	Z	Space group	Enthalpy (eV/atom)	ZPE (eV/atom)
1_bulk	12	*C*2/*c* SG 15	-3.347	0.014
2_bulk	6	*Cmmm* SG 65	-3.396	0.015
3_bulk	12	*Pnma* SG 62	-3.392	0.015

Table S7 Structural parameters of the proposed layered Te bulk allotropes (distances in Å, angles in °) within PBE functional with D2 correction.

Te	Z	Space group	Lattice parameter	Atomic coordination
1_bulk	12	*C*2/*c* SG 15	a=10.278, b=6.413, c=7.084 α=γ=90.0, β=117.1	8f (0.373 0.176 0.974) 4d (0.250 0.250 0.500)

2_bulk	6	*Cmmm* SG 65	a=8.238, b=6.036, c=4.105 α=β=γ=90.0	4g (0.766 0.500 0.000) 2d (0.500 0.500 0.500)
3_bulk	12	*Pnma* SG 62	a=7.554, b=4.153, c=13.346 α=β=γ=90.0	4c (0.966 0.250 0.375) 4c (0.826 0.250 0.064) 4c (0.938 0.750 0.215)

Table S8 The Te-Te distances around each $TeTe_m$ (m=3, 4, 5, and 6) centre and band gaps by the HSE06 functional in proposed one-, two- and three-dimensional covalent Te phases. In the bracket [m×n], the coordination number (m) and number (n) of $TeTe_m$ centres in the unit cell of each structure are presented. The shortest Te-Te distances between planar $TeTe_4$ and $TeTe_4$ centres in **3_bulk**, 2D **1** and **2** are also listed in italic.

Phases	Te-Te distances (Å), [m×n]	Band gap (eV, HSE06)
1_bulk	2.88-3.04(×3)/3.34-3.58(×2), [5×8] 3.04-3.05, [4×4]	0 (metallic)
2_bulk	3.00, [4×2] 3.00-3.03, [4×4]	0 (metallic)
$P3_121$ Te polymeric crystal	2.89(×2)/3.40(×4), [6×3]	0.326
3_bulk	2.84-2.99, [3×8] 2.99-3.01, [4×4] *3.89 ($TeTe_4$-$TeTe_4$)*	0.731
2D **3**	2.80-3.00, [3×4] 3.00, [4×2] *3.98 ($TeTe_4$-$TeTe_4$)*	0.951
2D **1**	2.75-3.04, [3×4] 3.03-3.04, [4×2]	1.388
2D **2**	2.76-3.02, [3×4] 3.02, [4×2] *4.20 ($TeTe_4$-$TeTe_4$)*	1.512

S8 Reference

1 A. R. Oganov and C. W. Glass, *J. Chem. Phys.,* 2006, **124**, 244704.
2 A. R. Oganov, A. O. Lyakhov and M. Valle, *Acc. Chem. Res.*, 2011, **44**, 227-237.
3 A. O. Lyakhov, A. R. Oganov, H. T. Stokes and Q. Zhu, *Comput. Phys. Commun.*, 2013, **184**, 1172-1182.
4 G. Kresse and J. Furthmüller, *Comput. Mater. Sci.*, 1996, **6**, 15-50.
5 G. Kresse and J. Furthmüller, *Phys. Rev. B*, 1996, **54**, 11169.
6 A. Jain, S. P. Ong, G. Hautier, W. Chen, W. D. Richards, S. Dacek, S. Cholia, D. Gunter, D. Skinner and G. Ceder, *APL Mater.*, 2013, **1**, 011002.
7 P. E. Blöchl, *Phys. Rev. B*, 1994, **50**, 17953.
8 J. P. Perdew, K. Burke and M. Ernzerhof, *Phys. Rev. Lett.*, 1998, **80**, 891.
9 J. P. Perdew, K. Burke and M. Ernzerhof, *Phys. Rev. Lett.*, 1996, **77,** 3865.
10 A. Togo, F. Oba and I. Tanaka, *Phys. Rev. B*, 2008, **78**, 134106.
11 M. Born and K.Huang, *Dynamical Theory of Crystal Lattices*, *Clarendon press*, 1954.
12 R. Cowley, *Phys. Rev. B*, 1976, **13**, 4877.
13 F. Mouhat and F.-X. Coudert, *Phys. Rev. B*, 2014, **90**, 224104.
14 Y. Le Page and P. Saxe, *Phys. Rev. B*, 2002, **65**, 104104.
15 C. Jasiukiewicz, T. Paszkiewicz and S. Wolski, *Phys. Status Solidi B*, 2008, **245**, 557-561.
16 J. Bardeen and W. Shockley, *Phys. Rev.*, 1950, **80**, 72.
17 Y. Xu, H. Zhang, H. Shao, G. Ni, J. Li, H. Lu, R. Zhang, B. Peng, Y. Zhu and H. Zhu, *Phys. Rev. B*, 2017, **96**, 245421.
18 D. Liu, X. Lin and D. Tománek, *Nano Lett.*, 2018, **18**, 4908-4913.